Mesozoic 003 (1): 074–084
https://www.mapress.com/mz/

Article

ISSN 3021-1859 (print edition)
MESOZOIC
ISSN 3021-1867 (online edition)

https://doi.org/10.11646/mesozoic.3.1.6
http://zoobank.org/urn:lsid:zoobank.org:pub:48D615CA-BA28-4998-9ED1-6535BE59259D

Testing the role of palaeolatitude in biotic recovery after the Permian–Triassic mass extinction: A palaeomagnetic comparison between South China and Oman

JUN-YUAN ZHOU[1, 2] & YONG ZHANG[1, 2, *]

[1]*State Key Laboratory of Palaeobiology and Stratigraphy, Nanjing Institute of Geology and Palaeontology, Chinese Academy of Sciences, Nanjing 210008, China*
[2]*University of Chinese Academy of Sciences, Beijing 100049, China*
jyzhou@nigpas.ac.cn; https://orcid.org/0000-0002-9691-3765
yzhang@nigpas.ac.cn; https://orcid.org/0000-0001-8237-6498
**Corresponding author*

Abstract

To evaluate whether palaeolatitude influenced spatial variations in biotic recovery following the end-Permian mass extinction, we conducted a palaeomagnetic comparison between two representative regions, South China and Oman, where contrasting recovery patterns have been documented. Detailed palaeomagnetic investigations were carried out in the Lower Triassic Yelang and Maocaopu formations in the Zunyi area of the South China Block. Characteristic remanent magnetizations (ChRMs) were isolated from 31 specimens across five sites (D_s = 224.4°, I_s = -10.5°, α_{95} = 6.7°). Rock magnetic measurements and scanning electron microscopy (SEM) observations indicate that the principal magnetic carriers are detrital magnetite and hematite. Together with the positive fold test, the ChRMs are interpreted as primary remanent magnetization acquired during deposition. This interpretation is further supported by the consistency of our results with other Early Triassic palaeomagnetic data from South China. The primary remanent magnetization directions yield a palaeolatitude of approximately 5°N for the Zunyi region in South China during the Early Triassic, placing it within the low-latitude Tethyan realm and comparable to coeval palaeolatitudes of Oman. These similar low-latitude settings suggest that latitudinal position alone is unlikely to have controlled the differences in biotic recovery between the two regions. Instead, other palaeogeographic factors, including the position relative to Pangaea and the consequent variations in ocean circulation, oxygenation state, and nutrient supply, may have played a more significant role in the spatial heterogeneity of Early Triassic ecosystem recovery.

Keywords: palaeomagnetism, Early Triassic, biotic recovery, palaeolatitude, South China

Introduction

The Permian–Triassic (P–T) transition represents one of the most profound biotic crises in Earth history, during which approximately 90% of marine species became extinct and global marine and terrestrial ecosystems were severely disrupted (Raup, 1979; Song *et al*., 2013; Fan *et al*., 2020). The subsequent Early Triassic represents a critical interval of ecosystem recovery; however, compared with other Phanerozoic mass extinctions, recovery was relatively protracted (Hallam, 1991; Erwin, 1998; Tong *et al*., 2007b). Increasing evidence indicates that biotic recovery during the Early Triassic exhibited pronounced regional variability (Roberts *et al*., 2025). For example, marine ecosystems in Oman developed relatively complex benthic communities within approximately 1–2 Ma following the extinction event, representing a comparatively rapid recovery mode (Twitchett *et al*., 2004). In contrast, multiple sections in South China record prolonged ecological impoverishment and simplified community structures that persisted through much of the Early Triassic, reflecting a typical ‘delayed recovery’ pattern (Tong *et al*., 2007a, b; Song *et al*., 2012). Together, these observations indicate that post-extinction ecosystem recovery was not a globally synchronous process, but was likely modulated by multiple regional environmental factors (Twitchett *et al*., 2004; Tong *et al*., 2007b; Luo *et al*., 2010; He *et al*., 2015; Song *et al*., 2018).

In the modern Earth system, latitude and its associated thermal belts exert a fundamental control on global ecological patterns. Biodiversity gradients, as well as rates of origination, extinction, and dispersal, are closely linked to latitude (Pianka, 1966; Willig *et al*., 2003; Mannion *et al*., 2014). Climate simulations suggest that although the latest Permian to Early Triassic interval was characterized by extreme greenhouse conditions, a temperature gradient still existed (Kiehl & Shields, 2005; Ragon *et al*., 2024). It follows that spatial differences in recovery rates may have been related to the latitudinal

 Submitted: 7 Mar. 2026; accepted by Z. Feng: 20 Mar. 2026; published: 30 Mar. 2026

temperature belts occupied by different regions. If this hypothesis is valid, regions exhibiting contrasting recovery patterns should have been situated within significantly different palaeoclimatic zones. Current understanding of Early Triassic environmental conditions in South China is derived primarily from geochemical and palaeontological evidence (*e.g.*, Tong *et al*., 2007a, b; Song *et al*., 2012; Song *et al*., 2014, 2018; Chen *et al*., 2015; He *et al*., 2015); however, quantitative constraints on the palaeolatitudinal positions of key regions remain comparatively limited. Palaeomagnetism provides a direct and independent means of reconstructing palaeolatitude. The primary remanent magnetization recorded at the time of rock formation can be used to determine palaeolatitude (Tauxe, 2010), thereby offering critical evidence for assessing whether regions with contrasting recovery patterns were located within significantly different climatic belts.

South China preserves continuous marine successions across the Permian–Triassic boundary that record environmental and biotic evolution before and after the extinction event (Yin *et al*., 1999, 2001). These successions provide an ideal natural archive for investigating the relationship between palaeogeography and biotic recovery. In Guizhou Province, extensive palaeontological and geochemical studies have documented the recovery patterns during the Early Triassic (*e.g.*, Tong *et al*., 2007b; Xiong *et al*., 2010; Chen *et al*., 2015; Dai *et al*., 2023). In this study, we conduct systematic palaeomagnetic, rock magnetic, and SEM analyses on the Lower Triassic Yelang and Maocaopu formations in the Zunyi area of Guizhou Province to obtain robust palaeolatitudinal constraints for South China during the Early Triassic. By integrating climate simulations and published palaeomagnetic data, we compare the palaeolatitudinal settings of Zunyi (South China) and Oman (Arabian) to evaluate whether latitude (and associated temperature) is sufficient to explain regional differences in Early Triassic biotic recovery. This study provides a quantitative palaeogeographic framework for understanding the mechanisms underlying ecosystem recovery following an extreme mass extinction event.

Geological setting

The South China Block lies in the southeastern part of East Asia and is bounded to the north by the Qinling-Dabie orogenic belt, to the southwest by the Indochina Block, and to the east by the Palaeo-Pacific domain (Meng & Zhang, 1999). It consists of the Yangtze and Cathaysia blocks, separated by the Jiangshao Fault Zone (Shu *et al*., 2021). Since the Late Palaeozoic, the South China Block has occupied the eastern margin of the Palaeo-Tethys Ocean and experienced long-lasting marine deposition under the combined influence of Pangaea assembly and subsequent rifting (Yin *et al*., 2014). Across the Permian–Triassic transition, South China developed a regionally continuous marine succession, which recorded the end-Permian mass extinction and the ensuing environmental and ecological reorganization, including major shifts in sedimentary systems, redox conditions, and biological communities (Payne *et al*., 2004; Tong *et al*., 2007b; Yin *et al*., 2014).

The sections investigated in this study are in the Zunyi area of the central South China Block (Fig. 1), where the Lower Triassic Yelang (T_1y) and Maocaopu (T_1m) formations are well exposed. During the Early Triassic, this region formed part of the shallow-marine siliciclastic shelf on the upper Yangtze Platform and hosts one of the best-preserved continuous marine successions in South China (Feng *et al*., 1997). The Yelang Formation comprises, from base to top, the Shabaowan Member (yellow-green shale with sparse fossils), the Yulongshan Member (thick micritic limestone rich in bivalves and gastropods), and the Jiujitan Member (purple-red silty mudstone with increasing bivalve abundance; Xiong *et al*., 2010). The overlying Maocaopu Formation (~450 m) transitions upward from bioturbated and dolomitic limestone representing open-marine to shallow-marine conditions to dolomite and dolomitic breccia deposited on a restricted carbonate platform, with more abundant and diverse fossil assemblages. Together, these strata record a prolonged Early Triassic ecological recovery in the Zunyi area, with fossil abundance generally increasing upsection throughout the Early Triassic succession (Xiong *et al*., 2010). Their continuous exposure, mixed carbonate-siliciclastic lithologies, and moderate deformation structures provide favourable conditions for preserving primary remanent magnetization and for conducting fold tests on characteristic remanent magnetization, providing an ideal natural archive for reconstructing palaeogeography and environmental evolution across the Permian–Triassic transition.

Material and methods

We conducted palaeomagnetic sampling of the Lower Triassic Yelang and Maocaopu formations in the Zunyi area. Five sampling sites were selected, including two from the Yelang Formation (ZY05 and ZY50) and three from the Maocaopu Formation (ZY03, ZY04, and ZY59). The sampled lithologies consist mainly of grey carbonates and purple-red silty mudstones, with minimal fracturing and no visible alteration or hydrothermal infilling. At each site, 5–10 cylindrical cores (2.5 cm in diameter) were drilled using a portable petrol-powered drill, yielding a total of 35 oriented cores. Core orientations were measured using both magnetic and sun compasses

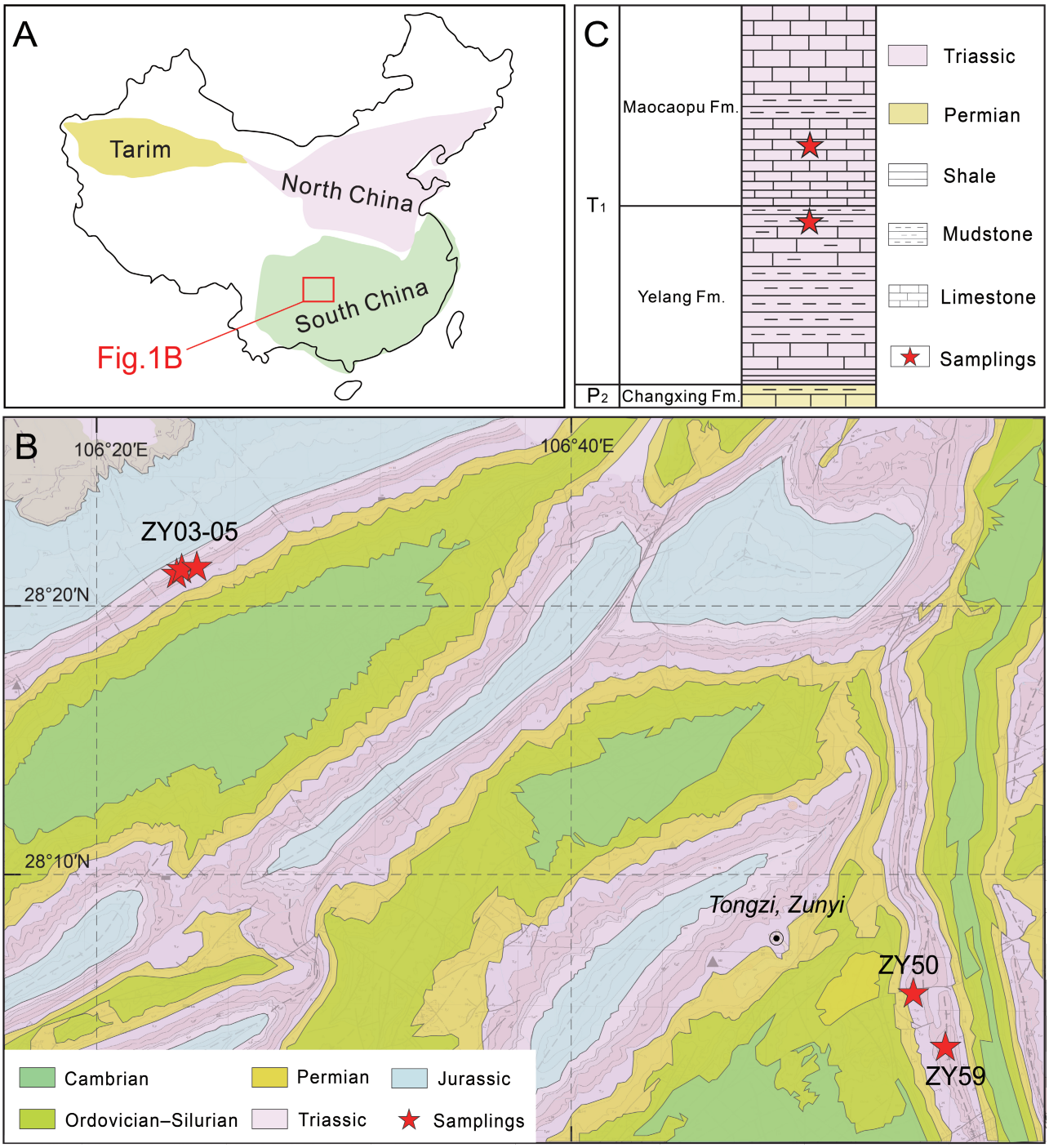

FIGURE 1. Geological setting, stratigraphic framework, and sampling sites of the Zunyi area in this study. **A**, Simplified map of the major blocks in China with our study area marked by a red square in South China. **B**, Simplified geological map of the Cambrian to Jurassic strata in Zunyi area and sampling sites are marked with red stars. **C**, The sketch stratigraphic column of the Zunyi area from P_2 to T_1, showing our sampling sites.

to minimize the influence of local magnetic perturbations. All samples were labelled in the field and transported to the laboratory for preparation and analysis.

In the laboratory, all oriented cores were cut into standard cylindrical specimens (2.5 cm in diameter, 2.2 cm in height) for palaeomagnetic and rock magnetic experiments. To isolate the characteristic remanent magnetization (ChRM), progressive thermal demagnetization was carried out inside a magnetically shielded room (ambient field <300 nT). Thermal demagnetization was performed using a TD-48 furnace with 50 °C intervals up to 250 °C and 30 °C intervals thereafter, to a maximum temperature of 690 °C. Remanence measurements at each temperature interval were conducted using a 2G-755R superconducting rock magnetometer at Nanjing University.

To determine the magnetic mineralogy, we performed rock magnetic analyses and SEM observations. Isothermal remanent magnetization (IRM) acquisition experiments were conducted on 5 representative samples using an ASC IM-10-30 impulse magnetizer and measured on an AGICO JR-6A spinner magnetometer. IRM acquisition curves were then unmixed using coercivity spectral analysis to distinguish magnetic minerals with different coercivity distributions (Kruiver et al., 2001). To further resolve the unblocking behaviour of magnetic components, we conducted triaxial isothermal remanent magnetization (Triaxial-IRM) experiments. In these experiments, following Lowrie (1990), samples were magnetized sequentially along three orthogonal axes, first Z (2.4 T), then Y (0.4 T), and finally X (0.12 T) allowing magnetic components of different coercivities to be partitioned into the three directions. During subsequent thermal demagnetization, the combined remanence acquired along these axes was demagnetized stepwise through the same temperature intervals used for ChRM isolation and the remanence was measured using the JR-6A magnetometer.

To characterize the microstructures and compositions of magnetic carriers, SEM imaging coupled with energy-dispersive spectroscopy (EDS) was conducted using a ZEISS Crossbeam 550 SEM with an OXFORD ULTIM MAX 170 EDS at the Nanjing Institute of Geology and Palaeontology, Chinese Academy of Sciences. Backscattered electron (BSE) images were obtained using 15 kV accelerating voltage, and EDS analyses were conducted with a probe diameter of <1 μm.

Results

Palaeomagnetic Results

The natural remanent magnetization (NRM) intensities of the samples range from approximately 3.43×10^{-4} to

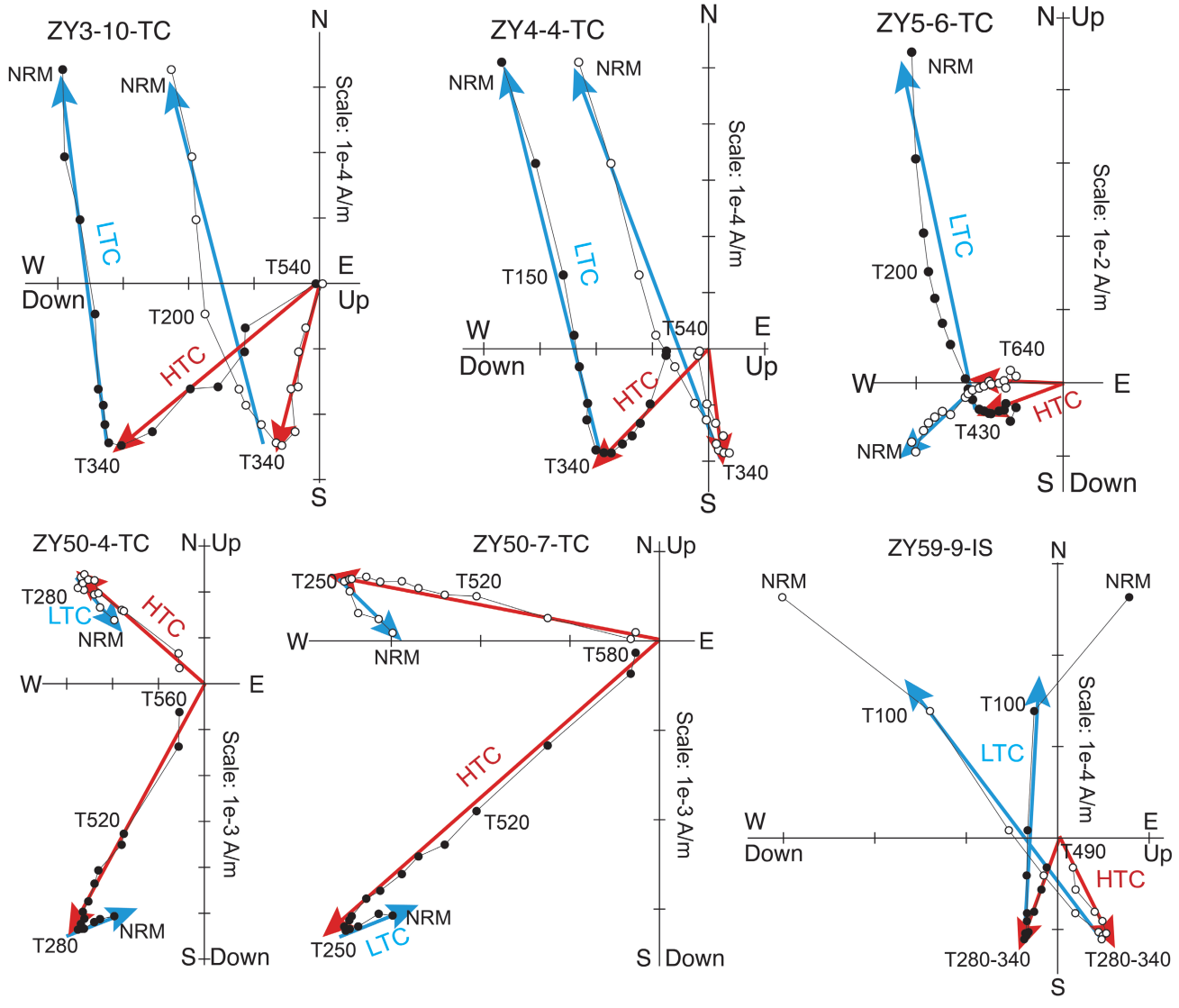

FIGURE 2. Progressive demagnetization plots of representative samples in this study. The blue line represents the LTC component, and the red line represents the HTC component.

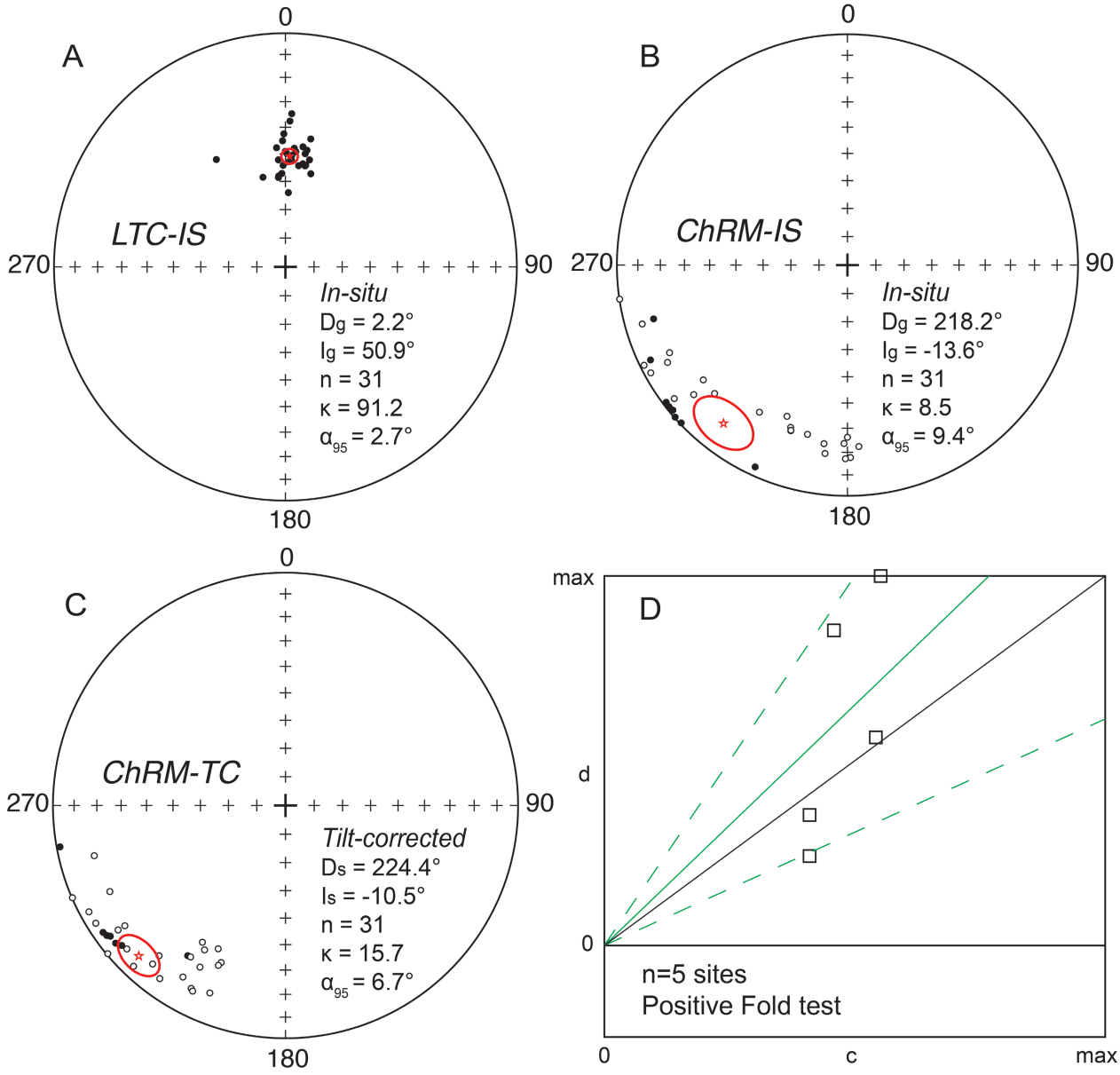

FIGURE 3. Palaeomagnetic results of the Early Triassic outcrops from Zunyi. **A**, Distribution of LTC directions in Equal-area stereographic projections in *in-situ* (IS) coordinates. **B**, **C**, The ChRM directions in Equal-area stereographic projections in *in-situ* (IS) and *tilt-corrected* (TC) coordinates, respectively. **D**, Fold test results.

8.96×10^{-2} A/m. Principal component analysis (PCA) of the stepwise demagnetization data reveals that most specimens contain two distinct components (Fig. 2). A low-temperature component (LTC) is typically removed below ~310–370 °C and yields a specimen-level mean direction of D_g = 2.2°, I_g = 50.9°, α_{95} = 2.7° (n = 31), which is consistent with the present-day geomagnetic field direction for the study area (Fig. 3A). A high-temperature component (HTC) is isolated between ~340 °C and ~580 °C and defines a stable characteristic remanent magnetization (ChRM). The site-mean direction of the HTC before tilt correction is D_g = 221.5°, I_g = -13.2°, α_{95} = 28.1° (n = 5). After tilt correction, the directions cluster more tightly, giving D_s = 225.6°, I_s = -9.9°, α_{95} = 18.6° (n = 5). Fisher statistics computed for all ChRM-bearing specimens similarly indicate well-grouped directions, with a specimen-level mean of D_g = 218.2°, I_g = -13.6°, α_{95} = 9.4° (n = 31) in geographic coordinates and D_s = 224.4°, I_s = -10.5°, α_{95} = 6.7° (n = 31) in tilt-corrected coordinates (Fig. 3B and C). A fold test based on the five site-mean directions shows a positive result (DC fold test; Fig. 3D; Enkin, 2003), indicating that the ChRM was acquired prior to folding. Using the tilt-corrected specimen mean direction, the corresponding virtual geomagnetic pole (VGP) position is calculated as λ = 42°, φ = 216.8°, with dp/dm = 3.4°/6.8°.

Rock Magnetic Results

IRM results indicate that the magnetic minerals in the samples are predominantly characterized by low to medium coercivities (Fig. 4A). For most samples (ZY03, ZY04, ZY50, ZY59), the IRM acquisition curves reach ~80% of the saturation remanence at ~200 mT, followed by a gradual increase and full saturation near ~800 mT. This behaviour suggests that low-coercivity magnetic minerals dominate these samples. For the sample from ZY05 site, the IRM curve also rises rapidly within the low–medium coercivity range, reaching ~80% of saturation at ~400 mT and increasing more slowly thereafter, but saturation is not achieved until ~2400 mT. This pattern indicates the presence of both low- and high-coercivity magnetic minerals. IRM acquisition curves were further analysed using coercivity unmixing (Kruiver et al., 2001). The results show that all samples contain two coercivity components. Samples from ZY03, ZY04, ZY50, and ZY59 sites exhibit two components with >85% of the IRM contribution from a low-coercivity fraction ($B_{1/2}$ = 40–80 mT, dispersion parameter Dp = 0.40), and a minor contribution (<10%) from a high-coercivity component. For ZY05, the IRM is divided into two nearly equal contributions (~50% each), with $B_{1/2}$ values of ~100 mT and ~316 mT and corresponding Dp values of 0.38 and 0.50, respectively (Table 2).

Triaxial-IRM experiments further support the coexistence of magnetic minerals with different

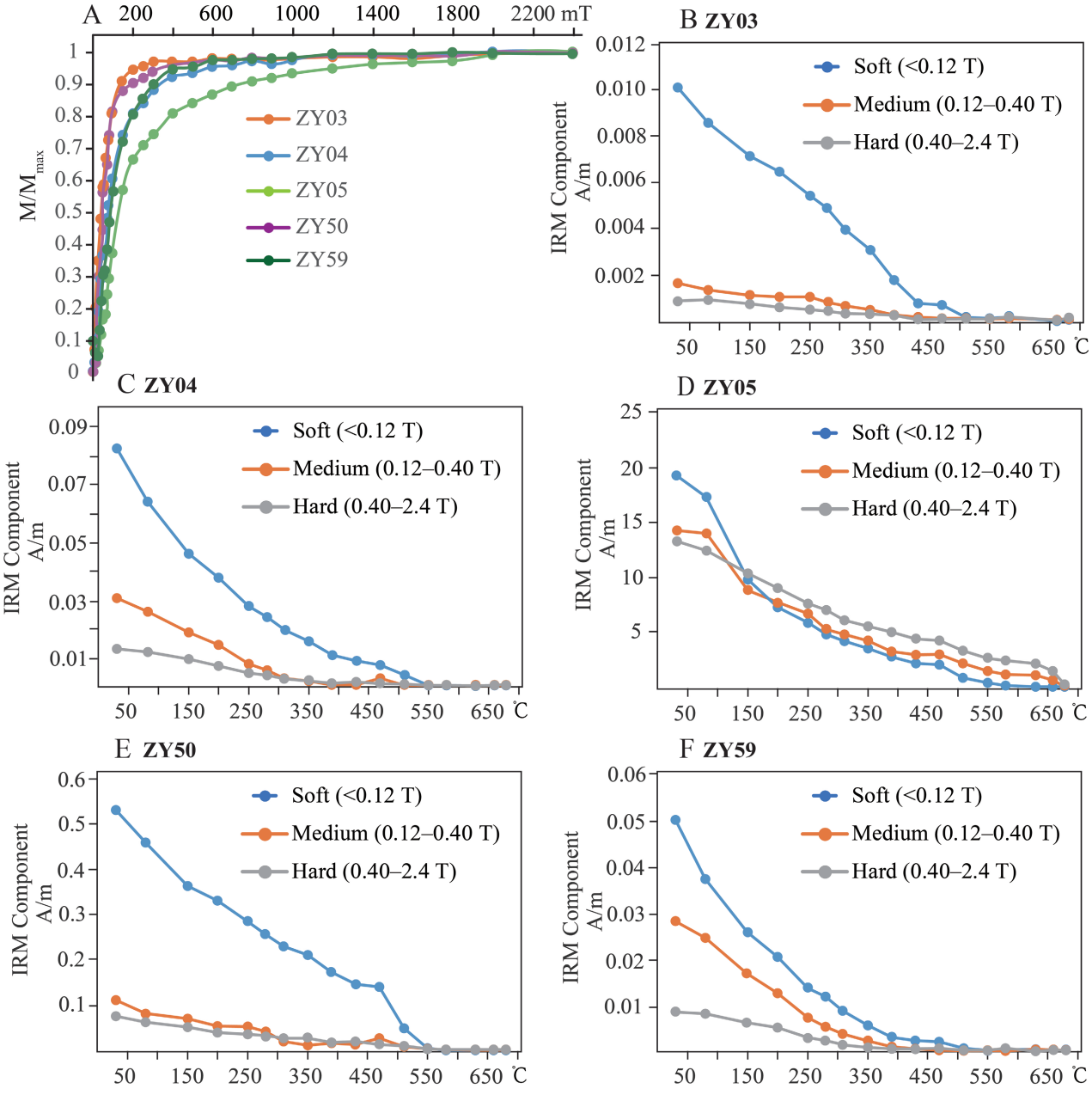

FIGURE 4. Rock magnetic results. **A**, IRM acquisition curves of representative samples. **B**–**F**, Triaxial-IRM thermal demagnetization curves of representative samples.

TABLE 1. Summary of palaeomagnetic results in this study.

Site	Stra.	S-Lon.	S-Lat.	S/D	N/N_0	D_g	I_g	D_s	I_s	κ	α_{95}
ZY03	T_1m	106°23′52″E	28°23′35″N	239/38	8/8	231.1	-5.4	229.5	0.6	25.9	11.1
ZY04	T_1m	106°23′52″E	28°23′35″N	239/38	6/8	234.9	-4.2	233.2	-0.8	27.1	13.1
ZY05	T_1y	106°23′58″E	28°23′28″N	238/44	5/5	250.3	-1.4	245.9	-9.5	55.1	12.5
ZY50	T_1y	106°54′16″E	28°06′07″N	21/52	8/9	186.6	-22.7	211.3	-24.7	55.7	7.0
ZY59	T_1m	106°55′44″E	28°04′16″N	352/26	4/5	198.3	-26.9	206.7	-13.5	434.2	4.4
Mean ChRM		Sites mean dir.		5 sites		221.5	-13.2	225.6	-9.9	18.5	18.6
		Specimens mean dir.		31 specimens		218.2	-13.6	224.4	-10.5	15.7	6.7
Palaeopole				~250 Ma		λ = 42°		φ = 216.8°		dp/dm=3.4°/6.8°	

Notes. S-Lat./S-Lon. are the latitude and longitude of sampling sites; N/N_0, number of specimens for mean direction calculation/ specimens demagnetized in each site; D_g, I_g, D_s and I_s, declination and inclination in geographic and stratigraphic coordinates; κ, precision parameter; α_{95}, 95% confidence circle.

TABLE 2. Results of the IRM Analysis Using the Method of Kruiver *et al.* (2001).

Site	Component	Contribution	Mean coercivity (mT)	Dp
ZY03	1	86	43.7	0.40
	2	14	6309.6	0.40
ZY04	1	92	72.4	0.45
	2	8	1000.0	0.50
ZY05	1	60	100.0	0.38
	2	40	316.2	0.50
ZY50	1	90	43.7	0.32
	2	10	398.1	0.50
ZY59	1	96	79.4	0.40
	2	4	1000.0	0.70

Notes. In the IRM acquisition analysis two components were identified. For each component, a contribution is calculated plus its mean coercivity and dispersion (Dp).

coercivities. In the purple-red silty mudstone at the site of ZY05, three coercivity components are present: a low-coercivity component that is essentially removed by ~580 °C, and medium- and high-coercivity components that decay to zero by ~680 °C. Samples from the remaining sites, which are all carbonates, display similar Triaxial-IRM patterns dominated by a low-coercivity component that is reduced to near zero by ~550 °C (Fig. 4B–F). Taken together, these observations indicate that magnetite is the primary magnetic carrier in the carbonate samples, whereas both magnetite and hematite contribute to the magnetization in the silty mudstone samples.

Microscopy and SEM Observations

Optical microscopy reveals that samples from most sites are dominated by calcite, and no clear evidence of late-stage fluid alteration is observed. The samples from the site of ZY05, by contrast, are purple-red silty mudstones containing abundant subangular detrital minerals such as quartz (Fig. 5A, B). Under reflected light, most magnetic grains appear as bright, angular particles, consistent with a detrital origin. Scanning electron microscopy further confirms these characteristics. Numerous angular detrital iron oxides are present in the silty mudstone samples (Fig. 5C–H), and no signs of chemical alteration or fluid-mediated replacement are observed along their grain boundaries. EDS analyses show that these grains consist primarily of Fe and O with minor Ti (Fig. 5I, J). A small number of acicular iron-oxide particles are also present, and their EDS spectra similarly indicate Fe and O as the main constituent elements.

Discussion

Palaeomagnetic analyses of the Lower Triassic limestones and siliciclastic rocks containing biotic recovery fossils in the Zunyi area of South China yield a well-defined ChRM. Both optical and electron microscopy demonstrate that the magnetic carriers are dominantly detrital

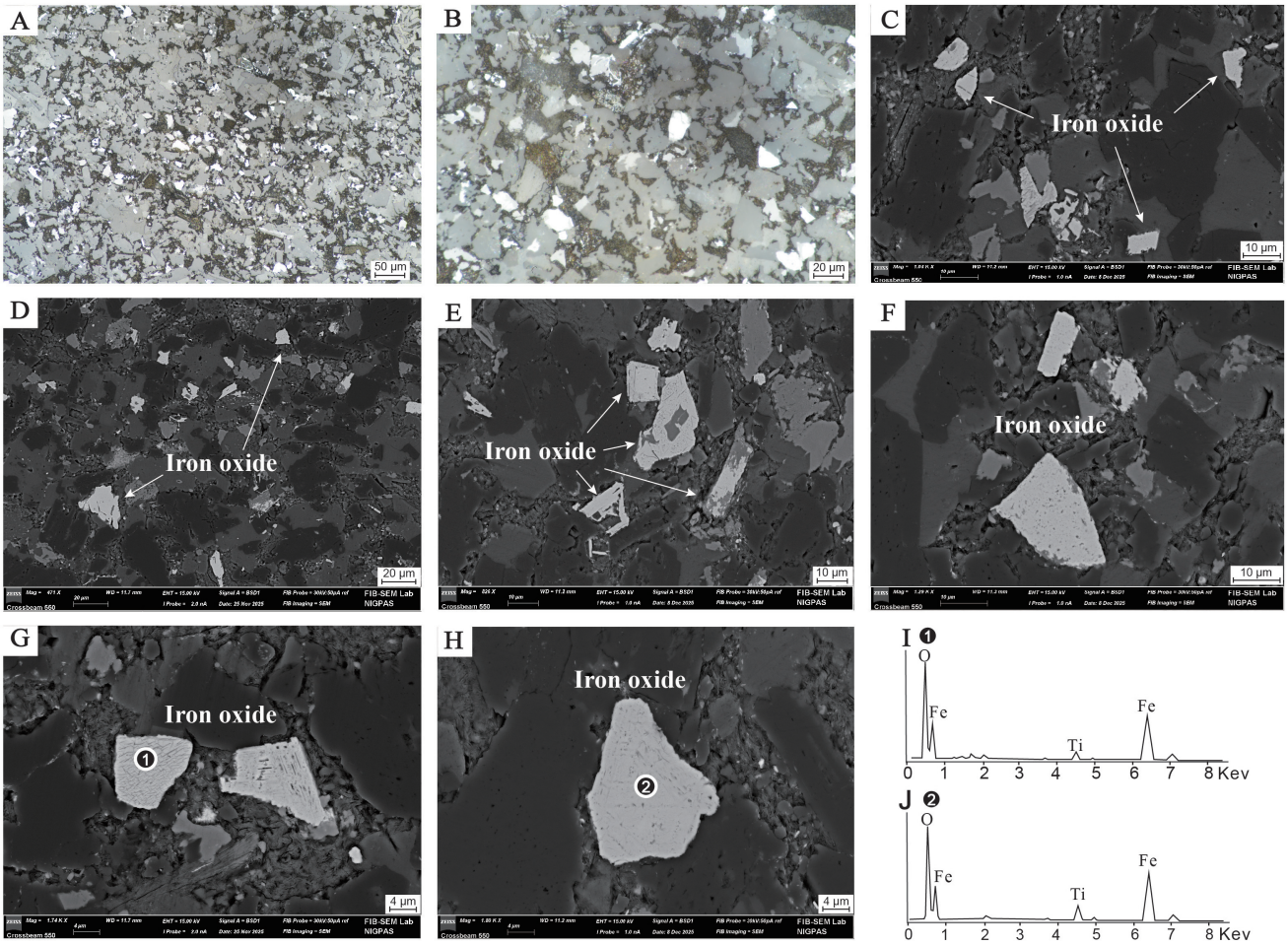

FIGURE 5. Microscopic and SEM photomicrographs of the representative samples. **A**, **B**, Reflected-light photomicrographs of silty mudstone showing magnetic minerals with well-preserved primary sedimentary textures and no evident mineralogical alteration. **C**–**H**, SEM images of silty mudstone illustrating the abundant occurrence of detrital magnetic minerals dispersed within the matrix. **I**, **J**, EDS spectra of representative magnetic minerals.

angular iron oxides that show no evidence of late-stage chemical overprinting, consistent with magnetite and hematite inferred from rock magnetic experiments. These observations establish a robust foundation for interpreting the remanence and its geological significance.

Timing of Remanence Magnetization Acquisition

We interpret the remanent magnetization in our samples as primary, acquired during Early Triassic deposition. Several lines of evidence support this conclusion. First, site-level directions pass the fold test of Enkin (2003), indicating that the magnetization predates Jurassic folding (Fig. 3). Second, the high-temperature components in most samples display negative polarity and decay toward the origin of demagnetization curves, with unblocking temperatures largely exceeding 550 °C (Fig. 2). Third, representative samples with stable ChRMs were examined using optical and scanning electron microscopy, revealing abundant sub-angular detrital magnetic grains with compositions corresponding to magnetite and hematite (Fig. 5). These grains show no signs of dissolution-reprecipitation or fluid-mediated alteration, further arguing against secondary acquisition. The Fisher-mean virtual geomagnetic pole calculated from the five site-mean directions ($\lambda = 42°$, $\varphi = 216.8°$, dp/dm = 3.4°/6.8°) closely matches previously published Early Triassic palaeomagnetic poles for the South China Block ($D_{kl} = 7.9$, $E^* = 0.19$; Heslop & Roberts, 2020; Fig. 6). Taken together, these lines of evidence strongly suggest that the ChRM recorded in the Zunyi section represents a primary remanent magnetization, faithfully preserving the geomagnetic field during the Early Triassic deposition.

Early Triassic Palaeolatitude of the South China Block

Given the primary nature of the ChRM, we use the tilt-corrected inclination to infer the Early Triassic palaeolatitude of the South China Block. The inclination corresponds to a palaeolatitude of ~5.3° ± 3.4° N/S,

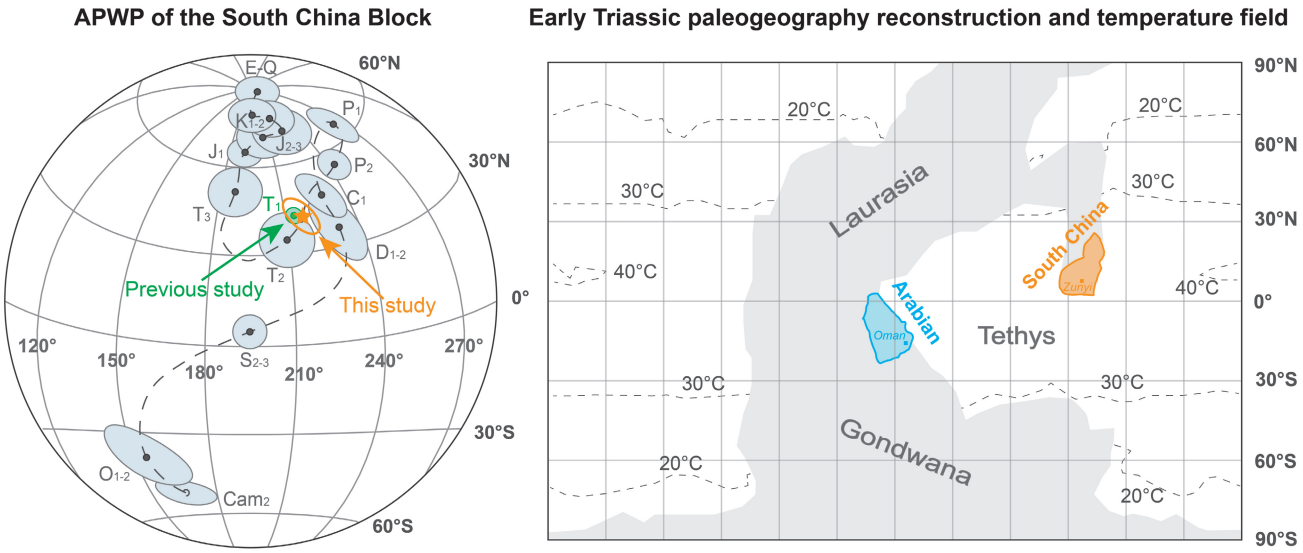

FIGURE 6. Apparent polar wander path (APWP) and palaeogeographic reconstruction of the South China Block and Arabian Block during the Early Triassic. The sea-surface temperature field is modified after Ragon *et al*. (2024).

placing Zunyi (South China) in a low-latitude equatorial position during the Early Triassic.

To evaluate the possible hemispheric placement, we consider the regional tectonic framework. During the Indosinian orogeny, South China collided with North China from east to west, forming the Qinling–Dabie orogenic belt. This tectonic scenario requires clockwise rotation of the South China Block. Under a Southern Hemisphere interpretation (D = 225.6°, I = -9.9°), the Early Triassic South China Block would have to rotate ~135° clockwise to reach its present-day orientation. Such a large-scale rotation is inconsistent with geological evidence and plate-kinematic reconstructions. In contrast, a Northern Hemisphere interpretation (D = 45.6°, I = 9.9°) requires only ~45° of counterclockwise rotation relative to present, or an equivalent ~45° clockwise rotation since the Early Triassic. This magnitude and sense of rotation are compatible with closure of the Palaeo-Tethys Ocean, continental-margin compression, and subsequent amalgamation of the South China, Indochina, and North China blocks (Zhang *et al*., 2015). This reconstruction is therefore more geologically and kinematically reasonable. We thus conclude that the South China Block resided at approximately 5°N within the Tethyan realm during the Early Triassic, positioned near the North China and Indochina blocks.

Implications for palaeolatitude control on biotic recovery

Our palaeomagnetic results indicate that the Zunyi area of the South China Block was located at a palaeolatitude of 5.3° ± 3.4°N during the Early Triassic, placing South China within the equatorial Tethyan realm. In comparison, published palaeomagnetic data from the central Arabian Plate indicate a palaeolatitude of ~12°S for the Early Triassic, from which we estimate a coeval palaeolatitude of ~15°S for Oman, situated along the northern margin of Gondwana on the southern shore of the Neo-Tethys (Torcq *et al*., 1997; Angiolini *et al*., 2003). Although a certain latitudinal difference existed between the two regions, both were located within the equatorial low-latitude tropical belt. Climate simulations indicate that such regions were characterized by persistently high sea-surface temperatures of ~30–40 °C and generally warmer than present conditions, accompanied by a reduced meridional temperature gradient (Kiehl & Shields, 2005; Ragon *et al*., 2024; Fig. 6). Therefore, within the 0–20° latitude range, temperature differences between regions would have been comparatively limited.

However, previous palaeontological studies have documented contrasting recovery patterns between Oman and South China, with relatively rapid ecosystem recovery in Oman and more prolonged ecological recovery in South China (Twitchett *et al*., 2004; Tong *et al*., 2007b). These differences suggest that palaeolatitude (and its associated temperature effects) alone is insufficient to account for regional variability in recovery patterns. Instead, regional palaeogeographic configuration, including continental arrangement, ocean circulation patterns, water-column stratification, oxygenation state, and nutrient supply, likely exerted a stronger influence on ecosystem recovery processes (Wignall & Hallam, 1993; Twitchett *et al*., 2004; Grasby *et al*., 2013; Song *et al*., 2014).

In summary, from the perspective of quantitative palaeolatitudinal constraints, regional differences in Early Triassic recovery rates more likely reflect variations in

palaeogeographic setting and marine environmental structure rather than simple latitudinal control.

Conclusion

Palaeomagnetic analyses of the Lower Triassic strata in this study indicate that the Zunyi area was located at approximately 5° N during the Early Triassic, placing it within the equatorial Tethyan realm. Comparison with coeval palaeomagnetic constraints from Oman suggests that both regions occupied similar low-latitude tropical environments. Despite these comparable palaeolatitudinal settings, marine ecosystems in the two regions experienced markedly different recovery patterns following the end-Permian mass extinction. This observation indicates that palaeolatitude and associated temperature gradients alone were unlikely to control regional differences in Early Triassic biotic recovery. Instead, variations in palaeogeographic configuration and ocean circulation, which affect oxygenation state and nutrient supply, likely exerted a stronger influence on ecosystem recovery dynamics.

Acknowledgments

This study was funded by the National Key Research and Development Program of China (2024YFF0807600), the National Natural Science Foundation of China (42272235 and 42288201) and the Fundamental Research Funds for NIGPAS (NGBS202209). We would like to express our gratitude to Xuzhi Hu, Qian Chen, Yunqian Jia and Tianhao Wu for their experimental assistance.

References

Angiolini, L., Balini, M., Garzanti, E., Nicora, A., Tintori, A., Crasquin, S. & Muttoni, G. (2003) Permian climatic and paleogeographic changes in northern Gondwana: The Khuff Formation of interior Oman. *Palaeogeography, Palaeoclimatology, Palaeoecology*, 191, 269–300. https://doi.org/10.1016/S0031-0182(02)00668-5

Chen, J., Tong, J., Song, H., Luo, M., Huang, Y. & Xiang, Y. (2015) Recovery pattern of brachiopods after the Permian–Triassic crisis in South China. *Palaeogeography, Palaeoclimatology, Palaeoecology*, 433, 91–105. https://doi.org/10.1016/j.palaeo.2015.05.020

Dai, X., Davies, J.H.F.L., Yuan, Z., Brayard, A., Ovtcharova, M., Xu, G., Liu, X., Smith, C.P.A., Schweitzer, C.E. & Song, H. (2023) A Mesozoic fossil lagerstätte from 250.8 million years ago shows a modern-type marine ecosystem. *Science*, 379, 567–572. https://doi.org/10.1126/science.adf1622

Enkin, R.J. (2003) The direction-correction tilt test: An all-purpose tilt/fold test for paleomagnetic studies. *Earth and Planetary Science Letters*, 212, 151–166. https://doi.org/10.1016/S0012-821X(03)00238-3

Erwin, D.H. (1998) The end and the beginning: Recoveries from mass extinctions. *Trends in Ecology & Evolution*, 13, 344–349.

Fan, J.X., Shen, S.Z., Erwin, D.H., Sadler, P.M., MacLeod, N., Cheng, Q.M., Hou, X.D. & Zhao, Y.Y. (2020) A high-resolution summary of Cambrian to Early Triassic marine invertebrate biodiversity. *Science*, 367, 272–277. https://doi.org/10.1126/science.aax4953

Feng, Z., Bai, Z., Wang, S., Li, Y. & Wang, G. (1997) Lithofacies palaeogeography of the Early and Middle Triassic of South China. *Chinese Journal of Geology*, 32, 212–220.

Grasby, S.E., Sanei, H., Beauchamp, B. & Chen, Z. (2013) Mercury deposition through the Permo-Triassic biotic crisis. *Chemical Geology*, 351, 209–216. https://doi.org/10.1016/j.chemgeo.2013.05.022

Hallam, A. (1991) Why was there a delayed radiation after the end-Palaeozoic extinctions? *Historical Biology*, 5, 257–262. https://doi.org/10.1080/10292389109380405

He, W.H., Zhang, K.X., Wu, S.B., Feng, Q.L., Yang, T.L., Yue, M.L. & Chen, B. (2015) End-Permian faunas from the Yangtze Basin and its marginal region: Implications for palaeogeographical and tectonic environments. *Earth Science*, 40, 275–289.

Heslop, D. & Roberts, A.P. (2020) Uncertainty propagation in hierarchical paleomagnetic reconstructions. *Journal of Geophysical Research: Solid Earth*, 125, e2020JB019488. https://doi.org/10.1029/2020JB019488

Kiehl, J.T. & Shields, C.A. (2005) Climate simulation of the latest Permian: Implications for mass extinction. *Geology*, 33, 757–760. https://doi.org/10.1130/G21654.1

Kruiver, P.P., Dekkers, M.J. & Heslop, D. (2001) Quantification of magnetic coercivity components by the analysis of acquisition curves of isothermal remanent magnetisation. *Earth and Planetary Science Letters*, 189, 269–276. https://doi.org/10.1016/S0012-821X(01)00367-3

Lowrie, W. (1990) Identification of ferromagnetic minerals in a rock by coercivity and unblocking temperature properties. *Geophysical Research Letters*, 17, 159–162. https://doi.org/10.1029/GL017i002p00159

Luo, G., Kump, L.R., Wang, Y., Tong, J., Arthur, M.A., Yang, H. & Xie, S. (2010) Isotopic evidence for an anomalously low oceanic sulfate concentration following end-Permian mass extinction. *Earth and Planetary Science Letters*, 300, 101–111. https://doi.org/10.1016/j.epsl.2010.09.041

Mannion, P.D., Upchurch, P., Benson, R.B.J. & Goswami, A. (2014) The latitudinal biodiversity gradient through deep time. *Trends in Ecology & Evolution*, 29, 42–50. https://doi.org/10.1016/j.tree.2013.09.012

Meng, Q.R. & Zhang, G.W. (1999) Timing of collision of the North and South China blocks: Controversy and reconciliation. *Geology*, 27, 123–126. https://doi.org/10.1130/0091-7613(1999)027<0123:TOCOTN>2.3.CO;2

Payne, J.L., Lehrmann, D.J., Wei, J., Orchard, M.J., Schrag, D.P. & Knoll, A.H. (2004) Large perturbations of the carbon cycle during recovery from the end-Permian extinction. *Science*, 305, 506–509. https://doi.org/10.1126/science.1097023

Pianka, E.R. (1966) Latitudinal gradients in species diversity: A review of concepts. *The American Naturalist*, 100, 33–46. https://doi.org/10.1086/282398

Ragon, C., Vérard, C., Kasparian, J. & Brunetti, M. (2024) Alternative climatic steady states near the Permian–Triassic boundary. *Scientific Reports*, 14, 26136. https://doi.org/10.1038/s41598-024-76432-8

Raup, D.M. (1979) Size of the Permo-Triassic bottleneck and its evolutionary implications. *Science*, 206, 217–218. https://doi.org/10.1126/science.206.4415.217

Roberts, A.J., Rucinski, M., Kear, B.P., Hammer, O., Engelschiøn, V.S., Scharling, T.H. & Hurum, J.H. (2025) Earliest oceanic tetrapod ecosystem reveals rapid complexification of Triassic marine communities. *Science*, 390, 722–727. https://doi.org/10.1126/science.adx7390

Shu, L., Yao, J., Wang, B., Faure, M., Charvet, J., & Chen, Y. (2021) Neoproterozoic plate tectonic process and Phanerozoic geodynamic evolution of the South China Block. *Earth-Science Reviews*, 216, 103596. https://doi.org/10.1016/j.earscirev.2021.103596

Song, H., Tong, J., Algeo, T.J., Song, H., Qiu, H., Zhu, Y. & Kump, L.R. (2014) Early Triassic seawater sulfate drawdown. *Geochimica et Cosmochimica Acta*, 128, 95–113. https://doi.org/10.1016/j.gca.2013.12.009

Song, H., Wignall, P.B. & Dunhill, A.M. (2018) Decoupled taxonomic and ecological recoveries from the Permo-Triassic extinction. *Science Advances*, 4, eaat5091. https://doi.org/10.1126/sciadv.aat5091

Song, H., Wignall, P.B., Tong, J. & Yin, H. (2013) Two pulses of extinction during the Permian–Triassic crisis. *Nature Geoscience*, 6, 52–56. https://doi.org/10.1038/ngeo1649

Song, H., Wignall, P.B., Tong, J., Bond, D.P.G., Song, H., Lai, X. & Chen, Y. (2012) Geochemical evidence from bio-apatite for multiple oceanic anoxic events during the Permian–Triassic transition and their link with end-Permian extinction and recovery. *Earth and Planetary Science Letters*, 353–354, 12–21. https://doi.org/10.1016/j.epsl.2012.07.005

Tauxe, L. (2010) *Essentials of Paleomagnetism*. University of California Press, Berkeley, California, 512 pp. https://doi.org/10.1525/9780520946378

Tong, J., Zhang, J., & Chen, Z.Q. (2007a) Early Triassic carbon isotope excursions from South China: Proxies for devastation and restoration of marine ecosystems following the end-Permian mass extinction. *Geological Journal*, 42, 371–389. https://doi.org/10.1002/gj.1084

Tong, J., Zhang, S., Zuo, J. & Xiong, X. (2007b) Events during Early Triassic recovery from the end-Permian extinction. *Global and Planetary Change*, 55, 66–80. https://doi.org/10.1016/j.gloplacha.2006.06.015

Torcq, F., Besse, J., Vaslet, D., Marcoux, J., Ricou, L.E., Halawani, M. & Basahel, M. (1997) Paleomagnetic results from Saudi Arabia and the Permo-Triassic Pangea configuration. *Earth and Planetary Science Letters*, 148, 553–567. https://doi.org/10.1016/S0012-821X(97)00047-2

Twitchett, R.J., Krystyn, L., Baud, A., Wheeley, J.R. & Richoz, S. (2004) Rapid marine recovery after the end-Permian mass-extinction event in the absence of marine anoxia. *Geology*, 32, 805–808. https://doi.org/10.1130/G20585.1

Wignall, P.B. & Hallam, A. (1993) Griesbachian (earliest Triassic) palaeoenvironmental changes in the Salt Range, Pakistan and southeast China and their bearing on the Permo-Triassic mass extinction. *Palaeogeography, Palaeoclimatology, Palaeoecology*, 102, 215–237. https://doi.org/10.1016/0031-0182(93)90068-T

Willig, M.R., Kaufman, D.M. & Stevens, R.D. (2003) Latitudinal gradients of biodiversity: Pattern, process, scale, and synthesis. *Annual Review of Ecology, Evolution, and Systematics*, 34, 273–309. https://doi.org/10.1146/annurev.ecolsys.34.012103.144032

Xiong, X.Q., Huang, Y.F. & Tong, J.N. (2010) Triassic bivalve biostratigraphic sequence in Zunyi, Guizhou Province. *Geological Science and Technology Information*, 29, 7–14.

Yin, H., Jiang, H., Xia, W., Feng, Q., Zhang, N. & Shen, J. (2014) The end-Permian regression in South China and its implication for mass extinction. *Earth-Science Reviews*, 137, 19–33. https://doi.org/10.1016/j.earscirev.2013.06.003

Yin, H.F. (1999) South China defined as part of the Tethyan archipelagic ocean system. *Earth Science*, 24, 1–12.

Yin, H.F., Zhang, K.X., Tong, J.N., Yang, Z.Y. & Wu, S.B. (2001) The global stratotype section and point (GSSP) of the Permian–Triassic boundary. *Episodes*, 24, 102–114. https://doi.org/10.18814/epiiugs/2001/v24i2/004

Zhang, Y., Jia, D., Shen, L., Yin, H.W., Chen, Z.X., Li, H.B., Li, Z.G., & Sun, C. (2015) Provenance of detrital zircons in the Late Triassic Sichuan foreland Basin: Constraints on the evolution of the Qinling Orogen and Longmen Shan thrust-fold belt in central China. *International Geology Review*, 57, 1806–1824. https://doi.org/10.1080/00206814.2015.1027967